Development of an Aeroballistic Range Capability for Testing Re-Entry Materials

G. D. Norfleet,* R. E. Hendrix,† R. M. Raper,‡ and E. E. Callens Jr.§
ARO, Inc., Arnold Air Force Station, Tenn.

Concentrated efforts in such areas as model launching techniques, test environment simulation, and specialized instrumentation have resulted in the emergence of the AEDC-VKF 1000-ft Hyperballistic Range (G) as a viable and versatile facility for testing re-entry materials. Its launch capability, long flight length, variable pressure capability, specialized instrumentation, and capability to provide several types of erosive test environments (e.g., rain, dust, snow) make Range G well suited for ablation, erosion, and heat-transfer testing. Eight laser photographic systems and three image-converter camera, photopyrometry systems provide in-flight measurements of nose-tip recession and surface temperature. These measurements, along with others characterizing the erosive environments, provide the primary data, and use of specially developed analytical procedures and testing techniques allow thorough evaluation of various materials as candidates for re-entry vehicle applications.

I. Introduction

THE thorough evaluation of materials selected as candidates for external surfaces of re-entry vehicles requires clean air ablation, erosion, and heat-transfer testing in ground-based test facilities. In order to obtain ground test data that are directly applicable to the re-entry flight case, it is necessary to duplicate rather than just simulate important aspects of the re-entry environment. For example, in obtaining materials data applicable to re-entry vehicles with large ballistic coefficients, a major problem is to duplicate simultaneously encounter velocity, stagnation enthalpy and stagnation pressure corresponding to a point in the re-entry trajectory. The significant advantage of the aeroballistic range in this regard is discussed by Grabowsky[1] and is illustrated in Fig. 1 (1970 data). Specifically, the aeroballistic range has this desired capability to duplicate simultaneously the very high levels of stagnation enthalpy and pressure at Mach numbers corresponding to the peak heating portions of re-entry trajectories.

In order to acquire meaningful data under these realistic test conditions, a state-of-the-art technology has been developed in Hyperballistic Range (G) to overcome problems associated with the severe model launch and free-flight environment, the short test time, and the acquisition of data from a hypervelocity test article. In particular, this advanced technology is manifest in the following developments: 1) model/sabot packages suitable for ablation, erosion, and heat-transfer testing; 2) instrumentation systems for erosive environment characterization; 3) instrumentation systems for measuring material response to the aerothermal and erosive environments; and 4) advanced data reduction hardware and techniques.

Presented as Paper 74-609 at the AIAA 8th Aerodynamic Testing Conference, Bethesda, Maryland, July 8-10, 1974; submitted August 19, 1974; revision received November 7, 1974. The research reported herein was conducted by the Arnold Engineering Development Center, Air Force Systems Command. Research results were obtained by personnel of ARO, Inc., contract operator at AEDC. Further reproduction is authorized to satisfy needs of the U.S. Government.

Index categories: Research Facilities and Instrumentation; Material Ablation; Hypervelocity Impact.

*Manager, Aeroballistics Branch, von Karman Gas Dynamics Facility (VKF). Member AIAA.

†Supervisor, Range Instrumentation Section, Aerospace Instrumentation Branch, VKF.

‡Project Engineer, Aeroballistics Branch, VKF.

§Research Engineer, Aeroballistics Branch, VKF. Member AIAA.

The purpose of this paper is to discuss briefly these developments and the resulting capability of the AEDC-VKF Range G for testing re-entry materials.

II. Experimental Technique

Range G is equipped with a 2.5 in.-caliber, two-stage, power-hydrogen gun approximately 150 ft long. The test range is a 1000 ft long, 10 ft-diam tube in which pressure can be maintained at any level from a few microns to 1 atm. The maximum obtainable test velocity is dependent upon the model weight, but models weighing 150 gm are routinely launched at velocities up to 20 kft/sec. Ablation tests have been conducted at average stagnation pressures of over 250 atm. Several types of test environments can be provided for material erosion studies: 1) rain fields consisting of approximately 1 mm-diam raindrops; 2) dust fields consisting of dust particles of various sizes and materials; and 3) snow fields consisting of dendritic-crystal snowflakes. The snowflakes are grown in the range on liquid-nitrogen-cooled plates and shaken loose at the desired time by a mechanical shock device. These features—launch capability, long flight length, variable pressure capability, capability to provide several types of test environments, and specialized instrumentation—make Range G well suited for ablation, erosion, and heat-transfer testing.

A. Model/Sabot Development

Design and fabrication of test models for use in the ballistic range is a difficult and demanding task because of the severity

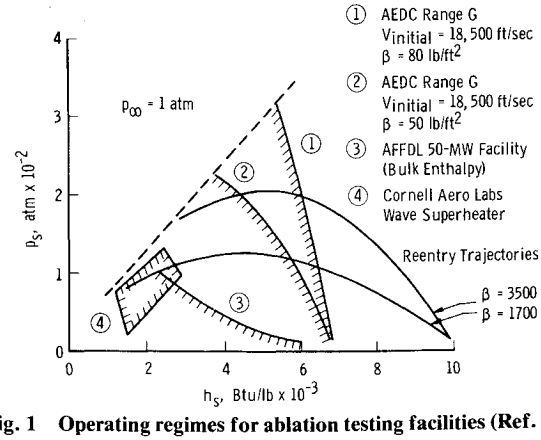

Fig. 1 Operating regimes for ablation testing facilities (Ref. 1).

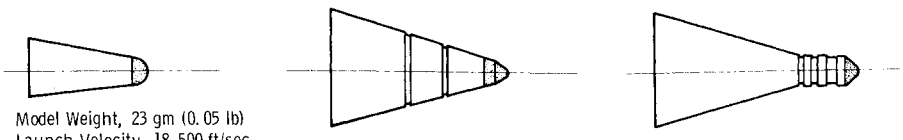

Model Weight, 23 gm (0.05 lb)
Launch Velocity, 18,500 ft/sec
β, 23 lb/sq ft
Launch Success, 50 percent
Overall Success, 0

Model Weight, 145 gm (0.32 lb)
Launch Velocity, 18,500 ft/sec
β, 70 lb/sq ft
Maximum Pressure for Full-Range Notch Survival - up to 1/3 atm
Launch Success, 59 percent
Overall Success, 55 percent

Model Weight, 155 gm (0.34 lb)
Launch Velocity, 18,500 ft/sec
β, 98 lb/sq ft
Maximum Pressure for Full-Range Notch Survival - up to 1 atm
Launch Success, 73 percent
Overall Success, 70 percent

Fig. 2 Development history of Range G ablation model.

of conditions existing during launch as well as in flight. As the model is accelerated to the desired test velocity, it must withstand acceleration levels of up to 250,000 g. The model and sabot must be separated with no significant model disturbance if it is to fly the full length of the range without unacceptable deviation from the range centerline and with only a small oscillatory angular amplitude. During flight the model must not ablate excessively, except over the surface of the test material, in order to maintain a set of resolvable reference dimensions for data reduction purposes. In addition, the ballistic coefficient must be large in order to minimize timewise variation in test conditions. These requirements were satisfied for ablation/erosion test applications by the development of a model/sabot package which combined an open-base sabot with a heavy model.

Design of models used in the initial phase of the development effort was based on experience accumulated with models developed for aerodynamic and wake tests. This design has since evolved into a much refined and superior test article for ablation and erosion studies. The development history is depicted in Fig 2, where launch success is defined as the percentage of all such models launched that were launched with no apparent damage. Overall success means that adequate ablation data were obtained during the flight. The difference between the two for the most part is attributed to poor trajectory or in-flight model failure.

Other models have been developed for other types of testing related to the re-entry materials problem.[2] For example, a very blunt conical model having the capability to simulate boundary-layer edge conditions experienced on full-scale re-entry nose tips has been developed for making calorimetric heat-transfer measurements in flight (Fig. 3). Measurements of the instantaneous melt location on the surface of the calorimetric section provide temperature versus time information from which heating rates may be inferred using a two-dimensional (2-D) transient heat conduction analysis.

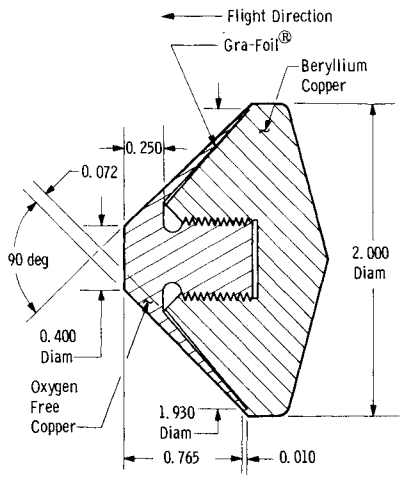

Fig. 3 45°, 0.400 diam flat face copper calorimeter model. (All dimensions in inches.)

B. Instrumentation

Range G is equipped with a variety of instrumentation for making routine operational measurements and also for producing special data as required during certain tests.[3,4] For testing re-entry materials, several special high-speed photographic systems are used to good advantage. Laser photographic systems are employed to provide model recession measurements; photographic pyrometry systems featuring image-converter cameras provide model surface temperature data; and other, more conventional, photography systems are used to provide detailed erosion field characteristics. These photographic systems employed during re-entry materials testing are described below.

Although not described here, X-ray, shadowgraph systems[4] are used to provide nose-tip recession data in those few cases where massive model erosion precludes meaningful interpretation of laser photographs. During certain metal ablation tests, for example, ablation material completely fills the reference grooves on the model (see Sec. IIC), obscuring them in the laser photographs. In such instances, X-ray shadowgrams, although of poorer optical quality than laser photographs, allow visualization of the reference grooves and measurement of nose-tip recession.

1) Laser photographic systems

Front-light laser photographic systems of the type shown in Fig. 4 have been developed which provide high-quality, stop-motion photographs of hypervelocity test models in the uprange portion of flight. Details of system operation are discussed in Refs. 5-8. Novel front-light/back-light laser photographic systems have been devised to provide the necessary coverage at downrange stations where model flight-path dispersion imposes stringent viewfield requirements. This technique employs several multi-lens cameras to provide at least one well-focused model photograph at each station and is described in Ref. 9.

The in-focus regions of the laser photographic system

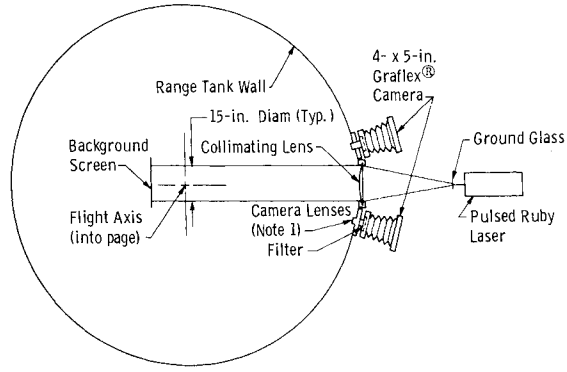

Fig. 4 Typical aeroballistic range front-light photographic system. Note: 1) each camera nominally has a total of four lenses. A staggered focus arrangement is employed to provide the required total depth-of-field. 2) Camera lens characteristics: focal length = 5.5 in., aperture = f/16. 3) Lenses are mounted so that they also serve as vacuum-tight windows.

viewfields were mapped with the aid of standard resolution charts via a technique described in Ref. 9. The optical resolution thus measured was on the order of 125 lines per inch or approximately 8 mils. For some camera lenses, 170 lines per inch or approximately 6 mils could be resolved.

A comment regarding optical resolution as it affects overall recession measurement accuracy is in order. Because of optical resolution limits and model motion (typically 4 mils) during the 20 nsec exposure time, the resultant photographic image of the model is blurred to some extent (although perhaps not apparent in the photographic examples shown here). In observing enlarged laser photographs, one tends to choose as the model edge a line of approximately constant film density, somewhere within this blurred region. A data reduction computer code (discussed in Sec. II c), has been formulated which addresses this problem both in terms of minimizing the measurement error and determining credible limits of the measurement uncertainty. The overall measurement uncertainty is, typically, 1-3 mils, a significant portion of which is directly attributable to optical resolution limits. As one might expect, then, the accuracy with which model dimensions can be measured somewhat exceeds the optical resolution as determined from standard chart measurements.

2) Photographic pyrometry systems

The concept of photographic pyrometry was envisaged as a means of providing the surface temperature measurements, and an innovative technique employing an image-converter camera was devised and successfully applied in Range G. [10,11] The technique involves basically the following sequence: 1) A high-speed, image-converter camera system is used to obtain a stop-motion, self-luminosity photograph of the test model in flight within Range G. Exposure times as short as 10 nsec can be obtained and exposure times of 100 nsec are typical of the Range G systems. 2) Calibration data from a carbon-arc reference source are recorded on identical film and are processed simultaneously with the model photograph. 3) Densities on the film image of the model surface are measured and converted to temperatures, using the calibration data.

Temperatures measured by this method are brightness temperatures, assuming that the radiation observed is strictly incandescent radiation. True surface temperatures may be calculated if the emissivity of the model material is known. In many instances, model materials of interest are carbon and graphite compounds with emissivities very near unity. In these cases, temperatures measured are representative of true surface temperatures (to within the measurement accuracy of the pyrometry systems).

The photographic pyrometry system is shown schematically in Fig. 5. The recording camera consists of an objective lens, an image-converter tube, a relay lens or fiber-optics face plate, and a film holder. Three photographic pyrometer systems are presently installed in Range G, and some pertinent characteristics of these systems are presented in Table 1.

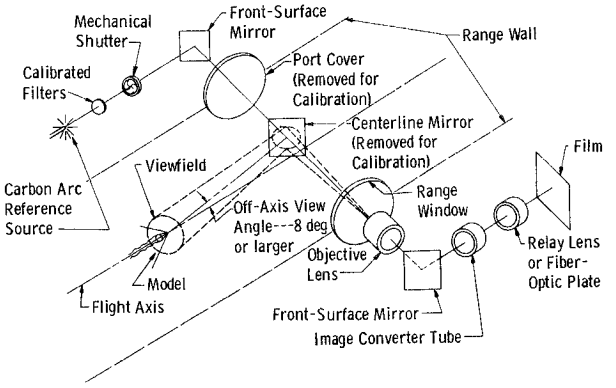

Fig. 5 Aeroballistic Range G photographic pyrometer system.

A direct analysis of system accuracy was conducted through static measurements of known temperatures as discussed in Ref. 11. These measurements were found to be within ±2% (±80 K) of the known value of 3806 ±10 K. t is felt that this assessment of accuracy, while made under static conditions, is indicative of the system accuracy which is realized during dynamic measurements of the brightness temperatures of aeroballistic range test models. The slight motion blur during range measurements should have an insignificant effect on temperature measurements, since this blur is considerably less than the optical resolution capability of the photographic pyrometry systems, as seen from Table 1.

3) Erosive environment photography systems

The mass of erosive material (snow, dust, rain, etc.) encountered by a hypervelocity test model must be known in order to evaluate thoroughly the effects of the encounter. Detailed erosion field characteristics such as number density and size are obtained from conventional front-light or backlight photographs. This information is then used, along with other experimental measurements correlating size and number density with mass, to provide data describing mass of erosive material encountered (see Sec. IIC). Both encountered mass and removed mass data are required to specify material performance.

The schematic of a front-light photographic system, using Xenon flash lamps as light sources, is shown in Fig. 6. This system is used to photograph individual planes of falling snowflakes a few milliseconds before model arrival. As in-

Table 1 Characteristics of improved Range G photographic pyrometry systems

Location (distance from range entrance), ft	System Description	I. C. Tube Resolution, mil	Objective Lens Focal Length, in.	Object Distance in.	Objective [a] Lens Magnification	Viewing Angle (from head-on), deg	Viewfield Diameter, in.	Exposure Time, nsec	Object Plane Motion Blur, [b] mil	Object [c] Plane Resolution, mil
210	2.5-in. -diam Abtronics I. C. camera with relay lens coupling to film	4	36	168	0.272	9	9.2	100	3	14.7
395	2.3-in. -diam Cordin I. C. camera with fiber optics coupling to film	3.3	24	168	0.167	9	13.8	10	0.3	19.8
593	5.0-in. -diam Abtronics I. C. camera with relay lens coupling to film	5	36	168	0.272	15	18.4	100	6	18.4

[a] Should not be confused with overall system magnification, does not include effect of relay lens.

[b] Based on model velocity of 18,000 ft/sec, viewing angles and exposure times as listed.

[c] Two points on the object, separated by this distance, can be unambiguously resolved in the final image. Values calculated from I. C. tube resolutions and objective lens magnification; effects of objective lenses and relay lenses on resolution are negligible in comparison with the limits imposed by I. C. tubes.

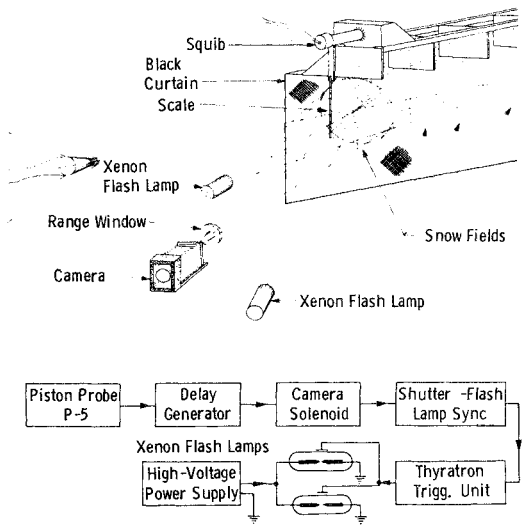

Fig. 6 Snow field photographic system. Shutter-Flashlamp Sync (contact closure) is provided after solenoid completely opens camera shutter.

dicated in Fig. 6, a pulse from a piston probe (in the pump tube of the two-stage launcher) is used to trigger a camera solenoid through a delay generator unit. Once the camera solenoid completely opens the camera shutter, a contact closure is provided which, in turn, triggers the flash lamps. The delay generator is properly adjusted so that the camera solenoid completes its entire sequence (shutter opening, exposure—flash lamp firing, and shutter closing) a few milliseconds before model arrival in the photographic viewfield. Twenty such systems using 270-mm focal-length camera lenses are presently installed in Range G; object plane resolutions of 0.006 in. are typical of these camera systems.

The primary uncertainties associated with determining the mass of snow or dust impacted are: 1) the error in estimating the mass in a specified reference area; 2) the error in assuming that the mass in the reference area is uniformly distributed; and 3) the uncertainty involved in measuring only a limited number of the snow or dust fields. The error in estimating the mass in the reference area is associated with the uncertainty in the correlation coefficient relating area and number of particles to mass. The mass distribution error is a result of the uncertainty in the location of the model penetration point. The error involved in measuring only a limited number of the fields is directly related to the axial mass variation. Typical values of the "one-sigma" uncertainties are shown in Table 2.

The uncertainties associated with dustfield measurements are considerably smaller than those associated with snow-field measurements because the dust particles are spherical and of known size and density, whereas the snowflakes are of irregular shape and variable size and density.

C. Data Reduction

In ablation and erosion testing, the primary data reduction task is the determination of nose-tip recession from in-flight laser photographs. This requires measurement of the length from the ablating or eroding surface to some reference plane and a scale factor to relate the image size to the actual model scale. The true and apparent contours are not necessarily the same (resolution and motion blur are discussed in Sec. II B, 1), and one must utilize all the available information presented in the image to establish the best statistical approximation to the true contour. The assumption that the apparent model edge is the actual model edge can lead to significant errors in nose recession measurements. The statistical analysis which has been applied to laser photograph measurements utilizes a series of equations to relate preflight and in-flight model dimensions through a scale factor and nose-tip recession terms. Reference dimensions obtained from the front and back of each groove and the groove diameters as seen in the side view of the model are least-squares fitted to the preflight dimensions to derive an estimate of the scale factor and its uncertainty. Lengths measured from the nose tip are treated similarly, yielding an estimate of nose-tip recession and measurement uncertainty. A computer program was developed to perform these computations for each photograph from which measurements are taken.

In-flight, self-luminosity photographs of the model nose tip obtained using the photographic pyrometry systems previously described constitute the basic data from which surface temperature information is inferred. The calibration negative and the data negative are processed simultaneously to minimize errors which might result from darkroom inconsistencies. The film densities associated with the developed negatives are digitized and recorded on magnetic tape by a digital scanning microdensitometer. These density data are then fed into a computer program which constructs density maps (lattices of discrete point measurements of density on the film images) of the model surface and the calibration spots. The known temperatures of the carbon-arc source are used in conjunction with density maps of the calibration spots to construct calibration curves of film density vs temperature. A computer program is utilized to generate isodensity contour maps of the model surface area of interest; and the calibration data are then used to label these density contours in terms of temperature, producing the desired isothermal map of the model surface.

The mass of snow or dust impacted is obtained from the conventional front-light photographs of the snow or dust fields (Fig. 6). A speical image analyzing computer system is used to obtain total snowflake projected area and number of flakes (or simply number of particles in the case of dust). This inforamtion is related to the corresponding total particle mass by an experimentally determined equation.

As previously described, the mass of nose material removed during the encounter with the snow field is evaluated from in-flight laser photographs (Fig. 7). The primary uncertainties associated with determining the mass of nose material removed are: 1) the profile measurement error; 2) the eroded volume error; 3) the hidden contour bias. The profile measurement error is a result of film response characteristics, motion blur, and finite optical resolution. The eroded volume error is associated with the determination of volume of material removed from a finite number of different two-dimensional profile views. The hidden contour bias results from the fact that depressions in the contour may be shielded from a profile view by adjacent surface elevations. Typical values of the "one-sigma" uncertainties are listed in Table 3.

Table 2 Typical Values of "one-sigma" uncertainties

Error source	Uncertainty nominal values, percent Snow	Dust
1) Correlation coefficient uncertainty	10	2
2) Penetration point uncertainty	14	4
3) Axial mass variation	6	2
Total mass impacted uncertainty	18	5

Table 3 Typical values of "one-sigma uncertainties

Error source	Uncertainty nominal values, percent Snow	Dust
1) profile measurement error	5	12
2) eroded volume uncertainty	13	9
3) hidden contour bias	8	2
Total mass removed uncertainty	16	15

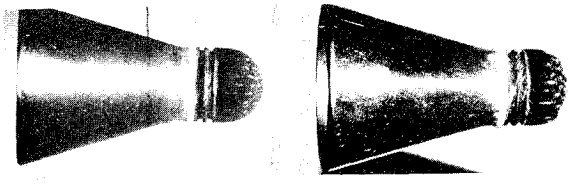

Fig. 7 Photography for snow erosion test in Range G. a) model before snowfield; b) model after snowfield.

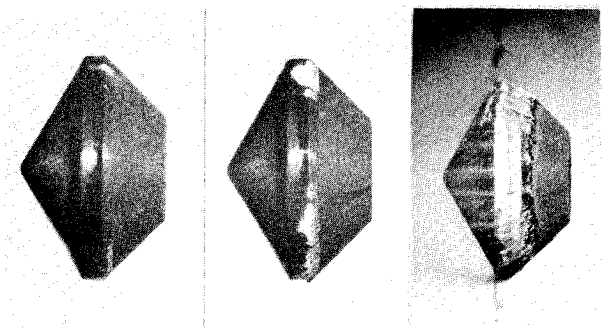

Fig. 8 Sequence of laser photographs illustrating melt line measurement technique.

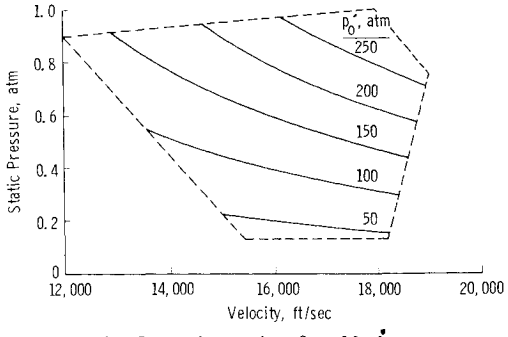

Fig. 9 Operating regime for ablation tests.

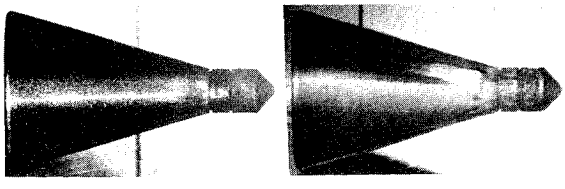

Fig. 10 Front-light laser photographs of Range G model; a) station 9—258 ft from muzzle; b) station 42—918 ft from muzzle.

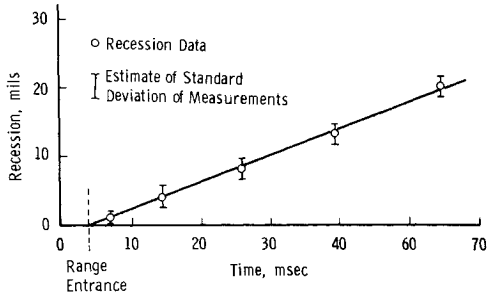

Fig. 11 Stagnation point recession data.

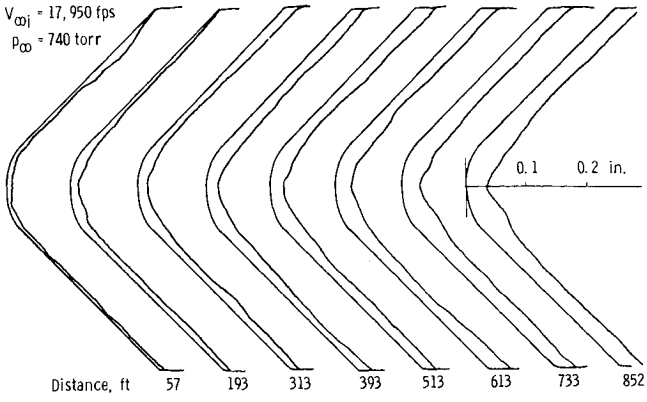

Fig. 12 Typical in-flight nose-tip profiles.

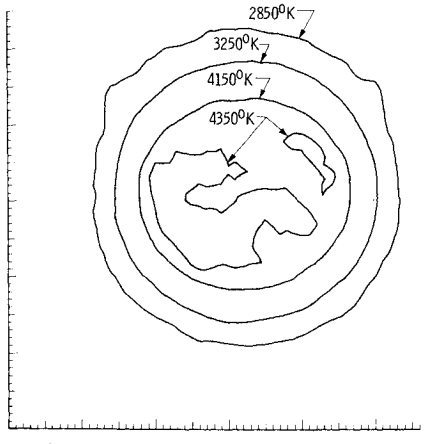

Fig. 13 Isothermal contour map.

Ablation (melting) of metals fabricated in special calorimeter models is readily discernible in the standard laser photographs and the locations of melt lines on the surfaces of these models can be studied as a function of flight distance via use of a series of laser photographic systems spaced along the model flight path (see Fig. 8). Heat-transfer data may thus be obtained by analyzing such a series of laser photographs. Heat-transfer data are also inferred from photopyrometry measurements of surface temperatures of high-temperature, nonablating models. Isothermal contours resulting from use of the photopyrometry systems provide information describing the location of boundary-layer transition and associated heat-transfer data.

III. Results

To date, ablation data have been obtained in Range G with several types of materials including various grades of bulk graphite, carbon phenolic, composite graphites, quartz phenolic, and high-temperature metals. More than 300 launches have been made over the relatively largest regime shown in Fig. 9. Sample front-lighted laser photographs for a typical graphite ablation shot are shown in Fig. 10. Stagnation point recession as a function of flight time for this shot is shown in Fig. 11. Several laser photographs from a similar shot were used to construct a series of in-flight profiles showing successive contour changes as shown in Fig. 12.

Another photograph of the model depicted in Fig. 10 is obtained from a near head-on position using one of the image-converter cameras. A contour map of the surface temperature data obtained from this photograph is shown in Fig. 13. A temperature profile taken through the centerline of the nose tip gives somewhat better spatial resoluton than does the contour map, as shown in Fig. 14, but this is only a consequence of the data presentation format.

The erosion tests conducted in Range G have been designed to evaluate the response at hypervelocity speeds of selected re-

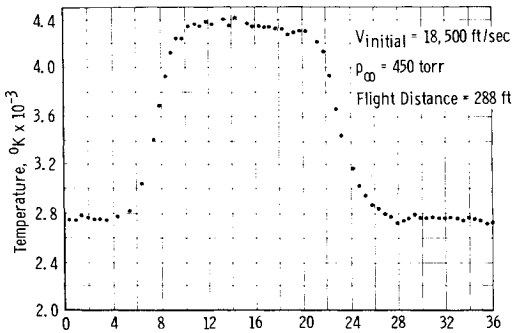

Fig. 14 Surface temperature profile; microdensitometer scan increment, microns $\times 10^{-2}$.

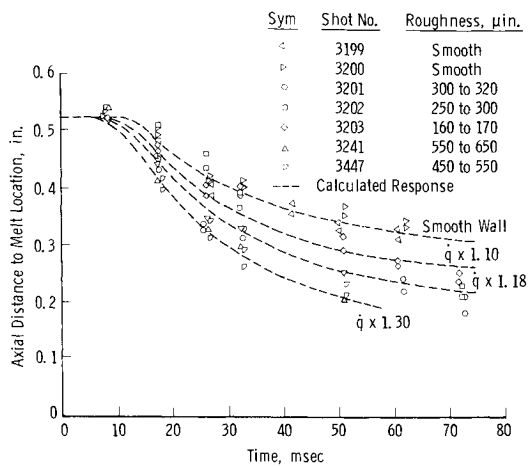

Fig. 15 Effect of surface roughness on calorimeter melt performance, $V_\infty = 15.5$ kfps, $p_\infty = 0.4$ atm, $\theta_c = 45°$.

entry vehicle nose-tip materials to simulated snow and dust fields. Eighty seven erosion launches have been made to date at nominal encounter velocities of 8, 12, 17 and 19 kfps and model stagnation pressures from 25 to 145 atm. The data presentation format is similar to that for ablation data.

Results obtained from a number of shots made using calorimetric heat-transfer models[2] are shown in Fig. 15. The objective of these tests was to evaluate the effect of surface roughness on heat transfer over a conical surface uninfluenced by entropy layer effects. The increase in heat transfer attributable to the roughened surface was inferred by iterating on the heat flux level input to a 2-D heat conduction computer code to find the percent increase in the smooth-wall values required to predict the observed performance. The results indicate that heating levels were increased approximately 30% over the smooth-wall level for the largest roughness height tested (mean roughness height of approximately 3 miles).

IV. Conclusion

Through the development of appropriate model/sabot designs, capabilities to produce erosive environments, specialized instrumentation and data reduction techniques, the AEDC-VKF Range G has emerged as a viable and versatile facility for testing re-entry materials and offers enthalpy and pressure duplication for most of the re-entry flight regimes of interest.

References

[1] Grabowsky, W. R., "Realistic Requirements for Present and Future Ground Testing Facilities," *Institute for Enviromental Sciences 16th Annual Technical Meeting and Equipment Exposition,* Boston, Mass., April, 1970.

[2] Raper, R. M., "Results of a Ballistic Range Test Program to Evaluate the Effect of Surface Roughness on Heat Transfer Utilizing a Calorimetric Model," AEDC-TR-73-161 (AD913562L), Sept. 1973, Arnold Engineering Development Corp., Arnold Air Force Station, Tenn.

[3] Hendrix, R. E. and Dugger, P. H., "Instrumentation for an Aeroballistic Range Test Facility," *ICIASF '73 Record*, Sept. 1973.

[4] Hendrix, R. E. and Dugger, P. H., "Photographic Instrumentation in Hyperballistics Range (G) of the von Karman Gas Dynamics Facility," *Photographic Applications in Science, Technology and Medicine,* Sept. 1973.

[5] Dugger, P. H., and Hill, J. W. "Laser Photographic Techniques for Direct Photography in an Aeroballistic Range," AEDC-TR-68-225 (AD683259), Feb. 1969, Arnold Engineering Development Corp., Arnold Air Force Base, Tenn.

[6] Dugger, P. H. and Hill, J. W., "A Laser Photographic System for Aeroballistic Range Photography," *ICIASF '69 Record,* May 1969.

[7] Dugger, P. H., et al., "Laser High-Speed Photography for Accurate Measurements of the Contours of Models in Hypervelocity Flight within an Aeroballistic Range," *Proceedings Electro-Optical Systems Design Conference*, New York, Sept. 1970.

[8] Dugger, P. H. and Hill, J. W., "A New Dimension in Front-Light Laser Photography," *AIAA Journal*, Vol. 10., Nov. 1972,pp. 1544-1546.

[9] Hill, J. W., "A Large Viewfield Laser Photographic System for Inflight Model Contour Measurements in an Aeroballistic Range," *Proceedings of the 18th National Aerospace Instrumentation Symposium*, Miami, Fla., May 1972.

[10] Dugger, P. H., et al., "A High-Speed Photographic Pyrometer," *Proceedings of Electro-Optics 1971 East Conference*, New York, Sept. 1971.

[11] Dugger, P. H., et al., "Photographic Pyrometry in an Aeroballistic Range," *Proceedings of the SPIE 16th Annual Technical Meeting*, San Francisco, Calif., Oct. 1972.